A Work on BAT and XRT Light Curves
Report on internship program

Martina Gerbino

Goddard Space Flight Center
Astrophysics Science Division, code 660

23th July - 23th September 2001

Contents

Part I

Overview of GRBs theory and observation

Chapter 1

Introduction

Gamma Ray Bursts (GRBs) are the most powerful phenomena in Universe. They are isotropic and very brief (from milliseconds to a few hundred seconds) gamma ray explosions. Their origin is still controversial, probably due to either massive stars collapse (Long GRBs) or neutron stars coalescence (Short GRBs). In this paper, some GRBs features are studied, in order to find correlations among GRB intrinsic properties. In particular, prompt emission and X band afterglow are analyzed. Data come from Swift satellite telescopes BAT and XRT. Sample is composed by only known redshift GRBs.

1.1   Project summary

The aim of this report is to summarize internship summer activity at Goddard Space Flight Center, Astrophysics Science Division, code 660. Internship program has dealt with Swift satellite data analysis, aiming to obtain further acknowledgements about Gamma Ray Bursts (GRBs) intrinsic properties.

Firstly, GRBs sample has been chosen. Looking for intrinsic properties, only GRBs with known redshift has been considered. This choice could likely exclude distance selection effects, looking up redshift distribution. The sample is composed by a hundred GRBs, selected from Gamma-ray Coordinates Network (GCN) archive (Circulars and Reports). The majority of them belongs to Long GRB classification: soft spectrum and particularly long emission, in contrast with Short GRBs (harder spectrum and very brief duration). Due to their longer last, Long GRBs are better analyzed than Short ones.

Following step has been to learn data analysis software manipulation. As this work focused on GRB prompt emission and X-band afterglow emission, data came from two of Swift satellite telescopes, such as Burst Alert Telescope (BAT, for prompt emission) and X-Ray Telescope (XRT, regarding afterglow). So far, software in use have been part of HEASoft (High Energy Astrophysics Software), namely FTOOLS and XANADU. Launching their pipelines, it has been possible to obtain weighted light curves and spectra, as far as sources

images.

Secondly, project has required a GRBs classification. Three main groups have been selected, observing BAT light curves. Classification item has been light curve feature, so the three groups are the following: single peak, multi peak and two events (belonging to the same observation, but separated by a conspicuous time lag). A positive correlation between BAT feature and XRT shape can be likely shown. As anticipated in previous lines, redshift distribution has been a key to exclude distance bias, being very homogeneous among the first two groups. Two-event group, actually, deserves a separated analysis, being very small sized and representing a particular class of events.

Third part of the project has been to look up more quantitative clues for such a correlation. Redshift-corrected light curves have been plotted, revealing expected results. Histograms of luminosity at chosen times for each group eventually show different GRBs distribution, revealing a promising result.

1.2 Paper structure

This paper is structured as follows:

1. PART 1 - It is a general part, dealing with GRBs theory and observation history. It is composed by 2 chapters:
   CHAPTER 2 - In this chapter, GRBs theory and observation are described. First section provides a GRBs overview; second section summarizes GRBs observation history; third part is about Swift satellite and its telescopes features.
   CHAPTER 3 - In this chapter, Swift analysis software are described. In particular, BAT and XRT software are reported, along with usage examples. Each of the two sections is structured in the same way: general overview about telescope measurements, pipeline description and results, such as sky images, light curves and spectra.

2. PART 2 - It is the bulk of this project. Data analysis and final results are reported in this part. It is composed by 3 chapters:
   CHAPTER 4 - In this chapter, sample choice and events classification are explained in detail.
   CHAPTER 5 - In this chapter, data corrections and final results are shown. First section describes what corrections have been necessary and why they have been applied; second section reports final plots and quantitative issues.
   CHAPTER 6 - In this chapter, work conclusion are listed.

Additional part is appendix, which sample dataset and classification groups are listed in. The paper ends with references.

Chapter 2

About GRBs and Swift

2.1 GRBs overview

GRBs [1] [2] [3] are the most powerful emission events in Universe. Their energy peak ranges from a few keV to MeV, that is soft gamma ray band. Multi frequency observation allows to identify two different components of GRBs emission: a prompt emission, that is GRB itself, and an afterglow, extending from X to optical and radio band. GRBs are very brief events, their duration lasting from milliseconds to a few hundred seconds. In contrast, afterglow tail could be very long, up to many days.

It is usual to classify GRBs in two main categories, long and short GRBs. Apart from obvious reference to duration, the former group shows softer spectra than the latter ones. This classification likely reflects two different GRBs progenitor categories. According to the most reliable hypothesis, long GRBs are emitted during massive stars collapse, which likely leads to black hole formation, while short GRBs could be echo spikes of two neutron stars coalescence. Obviously, short GRBs are more difficult to detect and, so far, to understand. For this reason, long GRBs theory and observation are more developed nowadays. Long GRBs detection in star formation regions and additionally identification of optical counterparts as Supernovae mostly stress fireball progenitor theory. According to it, prompt emission is due to shock wave propagation through internal stellar medium, with kinetic energy dissipation, while afterglow is produced by shock wave propagation through external interstellar medium.

GRBs luminosity is about $10^{51} - 10^{52}\,erg$ and this lets GRBs be the most energetic among known phenomena. It is known, though, that GRBs emission is particularly beamed. As a result, taking into account relativistic correction, luminosity lays on $10^{51}\,erg$, comparable with Supernovae luminosity.

2.2 GRBs observation history

July 2, 1967 detection of gamma ray emission is believed as first detection of a GRB . This event triggered detectors on board of Vela, a USA military satellite dedicated to sky survey, in order to identify potential nuclear weapon tests (during Cold War, URSS was believed to illegally test nuclear weapons, though Nuclear Test Ban Treaty signing in 1963). Vela was composed by four different satellite, with X-ray, Gamma-ray and neutron detectors on board. X and Gamma-ray events which triggered detectors, but were not observed by neutron ones, were carefully stored and destinated to future analysis.

The most popular explanation of GRBs initially involved Milky Way sources. However, launch of Compton Gamma Ray Observatory in 1991, with its Burst And Transient Source Explorer (BATSE) detector on board, revealed an isotropic distribution of GRB, allowing to exclude Galaxy sources (in this case, GRB distribution should be biased toward Galactic Plane).

2704 BATSE Gamma-Ray Bursts
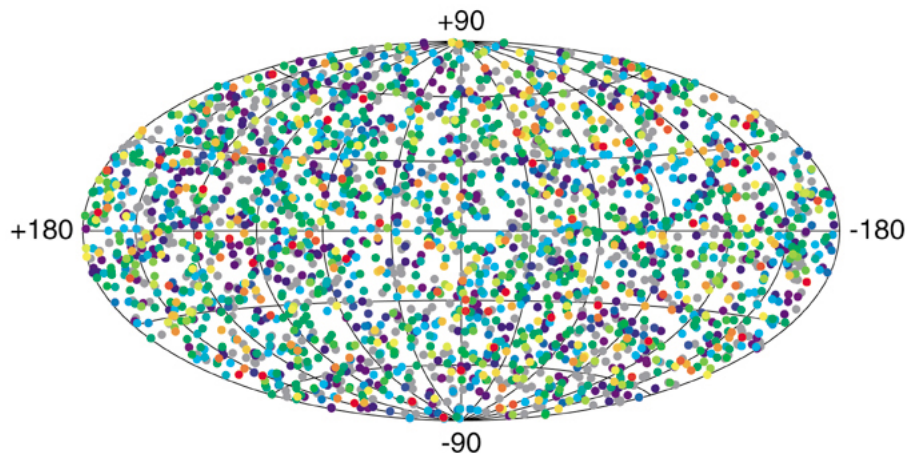
GRBs isotropic distribution as shown by BATSE detection.

Although GRB distribution was known, searching for counterparts had been unsuccessful until 1997, as BeppoSAX (launched in 1996) observed GRB970228 and its X-ray telescope detected a faint X-ray emission toward the same direction. After almost 20 hours, William Hershel Telescope noticed a very faint optical counterpart. As GRB faded, deep imaging was able to reveal a distant host galaxy. The first determination of host distance followed BeppoSAX discover of GRB970508 ($z = 0.835$), while the following year a bright Supernova ($SN1998bw$) was observed just a day after GRB980425 observation, toward the same direction. It was the first clue of link between GRBs and massive stars death.

During the following years, many dedicated instruments were developed in order to increase knowledge about GRB mechanism. In 2004, Swift was launched. It is a revolutionary satellite, able to rotate quickly as one of its telescopes detects a GRB. Recently, Fermi satellite was launched (2008): it can detect bursts with a hundred per year rate. Many of these bursts are bright enough to be analyzed by Fermi's Large Area Telescope (LAT). Apart from space missions, many ground-based observatories have been modified with the aim to observe optical counterpart as soon as GRB events are triggered by space telescopes and sent to ground-based telescopes by Gamma-ray Burst Coordinate Network (GCN).

2.3 Swift

Swift [4] is a very unique satellite, a multi-wavelength observatory for GRBs analysis. It is part of NASA's medium explorer (MIDEX) program and has been developed by a multinational collaboration among USA, United Kingdom and Italy. Swift was launched on November 20, 2004 into a low-Earth orbit on a Delta 7320 rocket.

It has three different telescopes on board, for performing multi-wavelength analysis of GRBs and afterglows in gamma, X, ultraviolet and optical bands. Burst Alert Telescope (BAT) triggers GRB events and determines GRB coordinates precisely. Within 90 seconds, spacecraft slews, pointing X-Ray Telescope (XRT) and UltraViolet and Optical Telescope (UVOT) toward the source. Swift name comes from this attitude to quickly rotate itself, a breakthrough in GRBs space missions.
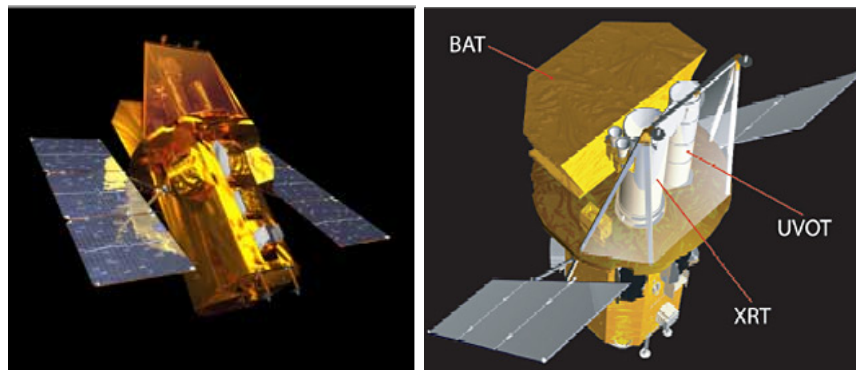
Swift satellite images. On the right, telescopes positions are shown.

As soon as BAT determines GRB position, coordinates are sent to ground-based observatories through GCN, aiming for optical counterparts and host galaxies images and distances. For some bursts, Swift is also able to calculate redshift by itself, using Lyman-α cut-off. As Swift data have been analyzed, free download from spacecraft website allows community to obtain them.

Many are Swift goals. Apart from known GRBs classification, the mission aims to identify new categories, study how GRBs evolve and influence surroundings, use them as tools for exploring early universe. Furthermore, Swift can perform the first sensitive hard X-ray sky survey.

2.3.1   Swift telescopes

As previously shown, Swift instruments are three telescopes, performing in three different wavebands: BAT, for gamma-ray prompt emission analysis, XRT and UVOT dedicated to X-ray and UV/optical afterglow analysis respectively. For this report aim, UVOT will be described more briefly than BAT and XRT.

2.3.1.1   BAT

Burst Alert Telescope is a high sensitive, large Field Of View (FOV) instrument, developed for triggering GRBs and determining their position within 4 arcminutes. It works in 15-150 KeV energy range and decides whether a burst could be significant to request a spacecraft slew. In case, BAT calculates burst position and sent it within seconds.

BAT is provided with a large dynamic range and trigger capabilities, so it can perform both bright and faint GRBs analysis. Two dimensional coded-aperture mask is the instrument bulk: it allows to analyze weak bursts, as the large FOV makes bright bursts detection possible. However, large FOV is also supposed to include X-ray and UV/optical FOV. As a result, long GRBs are followed up simultaneously by BAT, XRT and UVOT.

BAT structure is hierarchical: detector elements are assembled into arrays, modules and, finally, blocks. In such a way, loss of individual pixels does not invalidate the whole telescope operation. Coded-aperture mask, made by several lead tiles, uses a random 50%open-50%closed pattern, rather than the standard pattern, due to technical requests. The mask is surrounded by a shield against isotropic cosmic radiation and Earth albedo.

BAT software is provided with a Figure Of Merit (FOM), which allows to determine whether an observed burst is particularly interesting to request a spacecraft slew. FOM parameters can be modified or added to current ones. In addition to BAT signals, Swift can perform automatic observations, scheduled by ground-based team. Two are operation modes: burst mode, which provides burst identification and analysis, and survey mode, which executes hard X-ray all-sky survey. When operating in burst mode, a dedicated algorithm allows to identify GRBs, comparing burst counts with known background counts and thresholds. Imaging capability is a key, as it let to exclude any other similar results sources, requesting the source to be a point one.

2.3.1.2   XRT

X-Ray Telescope operates in 0.3-10 keV band and is able to perform source images and to calculate light curves and spectra. It can cover a very wide range

in flux, laying within almost 7 orders of magnitude. It focuses measured flux on a CCD-22 $600 X 602$ pixels detector.

XRT can operate in two states, Manual, for calibration, and Auto. Both the state allow 4 modes, which can be chosen automatically by the instrument. Imaging Mode provides a higher than BAT sensitivity image, integrating total energy deposited per pixel, so it can produce spectral information. Along with the brightest source, there are often some other sources in the same field of view. However, the brightest one is always GRB counterpart and its precise position is immediately sent to ground-based instruments for accurate followup. Photon-Counting (PC) mode produces both imaging and spectral results for flux sources up to $9\,10^{-10} erg\,cm^{-2}s^{-1}$. Any detected Fe line should be a tool for redshift determination within a 10% accuracy. Photodiode mode is used for very bright sources and for high time resolution; it has not spatial information, so it can only produce light curves and spectra. Window Time (WT) mode performs a serial register columns binning and it is useful for medium bright sources; it can also provide sky image. However, WT images are 1D ones.

2.3.1.3   UVOT

UltraViolet and Optical Telescope, based on XMM-Newton Optical Monitor (OM), can perform both images and spectra. Images provide a 0.5 arcsec source position. Spectra, obtained via a grism (combination of prism and grid) filter, allows to calculate redshift measuring Lyman-α cut-off.

Chapter 3

Data analysis software

As soon as an event is detected, raw data are sent to ground-based observatories. These raw data are analyzed by Swift Data Center (SDC), at Goddard Space Flight Center (GSFC). Three consequent analysis levels can be recognized. Level 1 creates FITS files containing images and event data from raw data; level 2 produces calibrated event data and images, after screening and coordinate transformation; finally, spectra, light curves and sky images come from level 3 analysis.

All data are available in UK, Italian and HEASARC (USA) archives [8].

For this report purpose, just BAT and XRT software are described [5]. Both of them required data download from archive, obviously, and initialization of CALibration DataBase (CALDB). To check whether CALDB is correctly installed, the following lines have to be typed:

> *caldbinfo*
> *Mode (BASIC, INST, or FULL)[ ] INST*
> *Name of Mission[ ] SWIFT*
> *Name of Instrument[ ] BAT*

If procedure works well, the following message appears below previous commands:

> *** caldbinfo 1.0.2*
> *... Local CALDB appears to be set-up & accessible*
> *** caldbinfo 1.0.2 completed successfully*

For didactical purpose, GRB091029, otherwise ID target 00374210000, data will be analyzed. Data have been downloaded from Quick Look USA website [8]. They include Auxil, BAT and XRT data.

3.1 BAT analysis

BAT analysis software is part of HEASOFT, known as FTOOLS. It is crucial to understand BAT instrument. As shown previously, BAT instrument is based on Coded Aperture: a lead mask, provided with a random but known pattern,

casts a shadow on a positive detector plane just below it, collecting light from sky sources. Obviously, many sources in the same field of view produce an integrated detector result. However, each source determines its own shadow onto detector, as a result of its own brightness and orientation. As mask pattern is known, a dedicated software is able to disentangle different sources shadows and to produce final point source image, moving from detector space to image space. Final result of this cross-correlation process is a mask-weighted flux for each position on the sky. Cross correlation involves multiply-and-sum operation between mask pattern and detector shadow: if a source is in a given sky position, then mask shadow is highly correlated with detector storage (excess of counts where mask is open, loss of counts where mask is blocked); otherwise, cross-correlation is very faint.
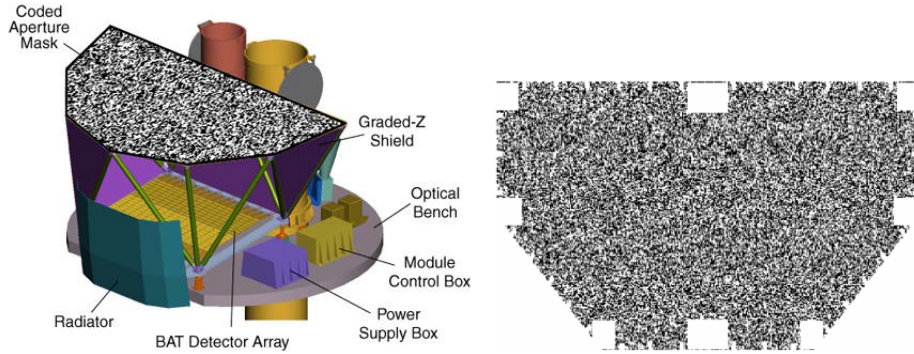
BAT telescope structure (left side) and a BAT mask zoom. The random pattern is clearly evident.

Standard analysis is possible using *batgrbproduct* script. However, user can make his own products using FTOOLS scripts. Standard steps in BAT analysis are the following:

- Making a detector quality map. Some detectors could have too many or too few counts respect to statistical fluctuation. Furthermore, some detectors could not be working because of restoring operations. For these reasons, a quality map is requested for all the following items.

- Mask weighting. This step is a key to obtain background-subtracted light curves, spectra and images. It converts each degree of shadowing into a weight. It has to be stressed that mask weighting operation is performed just for a single source. If user is interested in more sources in the same field of view, different mask weighting has to be performed for each one.

- Extracting light curve

- Extracting spectra

- Generating response matrix. It is part of spectrum corrections and applies just for a particular source position. For instance, if GRB prompt emission is detected during spacecraft slew, a single response matrix should not be applied for the whole emission range.

- Extracting sky image. This issue requires three consequent steps, involving reconstruction of flux at each detector point: making a source Detector Plane Image (DPI), making a background DPI, making sky image performing *batfftimage* script.

3.1.1 BAT pipeline

In this section, BAT scripts and results are reported. A complete and understandable guide can be found at UK Swift website [5].

3.1.1.1 Quality map, hot pixels and mask weighting

The following commands allow to produce files containing quality map, defining hot (that is not working) pixels and weighting final map.

- >*batbinevt*
  After typing this command, user is requested to insert input and output file name along with further analysis information. Input file is *swNNNNNNNNNNNNbevshsp_uf.evt* (in this case, N stands for 00374210000) and is located in *.../bat/event* directory. Output file name is *grb.dpi* here. If script works well, batbinevt environment opens. These are final lines:
  DPIs written to grb.dpi
  EBOUNDS written to grb.dpi
  Number of Rows Processed: 15054494
  Number Accepted/Rejected: 1.50537e+07/834
  Time Bins: 1 Energy Bins: 1

- >*bathotpix detmask=sw00NNNNNN000bdecb.hk.gz*
  The *.hk.gz* file is located in *.../bat/hk* directory (hk stands for housekeeping). User is requested to type input and output file name. Input file is previous *grb.dpi*. Output file is *grb.mask* here. If script works well, a report of hot pixels is shown on terminal.

- >*batmaskwtevt detmask=grb.mask*
  User is requested to enter input and attitude files, along with object coordinates in Right Ascension (RA) and DEClination (DEC). Coordinates can be found in *bevshsp_uf.evt* header, which can be opened typing *fv filename* (*filename* stands for **.evt* file name) on terminal shell. If script works well, at the end of batmaskwtevt environment a message showing number of processed events is wrote. This command does not create a new file, just correct hot pixels list.

3.1.1.2   Light curve and spectrum

As BAT energy range lays from 15 to 350 keV, light curves over any energy band into this interval and with any time bins can be obtained. This is the command:

> *batbinevt detmask=grb.mask*

It is the same command that results in **.dpi* file. In this case, user is requested to enter *lc* extenction. Energy ranges are also requested: here 4 ranges have been chosen, such as $15 - 25, 25 - 50, 50 - 100, 100 - 350\,keV$. Light curves can be shown using *fplot* command, choosing */xt* as terminal (that is X terminal). Additionally, to type *fcalc* command before creating light curves allows to set X axis as time after BAT trigger time.

A light curves plot for $GRB091029$ is reported below.
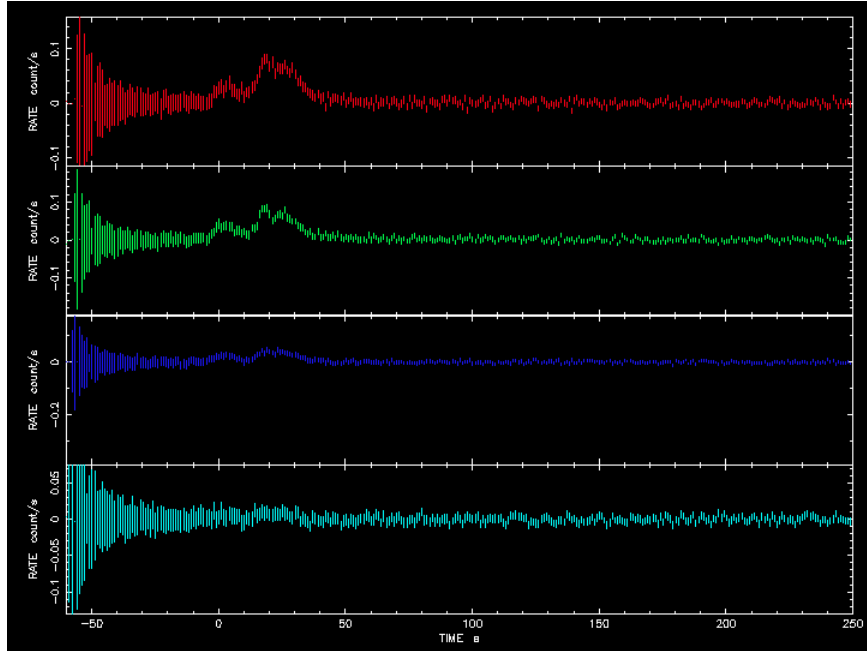
BAT light curves for $GRB091029$, for 4 different energy ranges. From top to bottom, $15 - 25, 25 - 50, 50 - 100, 100 - 350\,keV$. X axis has been setting so it shows time since BAT trigger time. Y axis reports count rate.

BAT spectrum can be obtained performing the following command:

> *batbinevt detmask=grb.mask tstart=# tstop=#*

where *tstart* and *tstop* can be chosen by user. The following command provides data sample starting and ending time:

> *fkeyprint sw00NNNNNN000bevshsp_uf.evt+0 tst*

Once spectrum has been created, there is a need for response matrix in order to fit it. To type *batdrmgen* in shell terminal allows to do that. Now, spectrum can be fitted using *XSPEC*. It has to be stressed that fit should be performed

between $15-150\,keV$: outside of this range, BAT detector becomes transparent to radiation.

Fitted spectrum and residuals plot for GRB091029 are shown below. These plots have been obtained using *XSPEC* commands. A usefull guide is available on the Web [10].
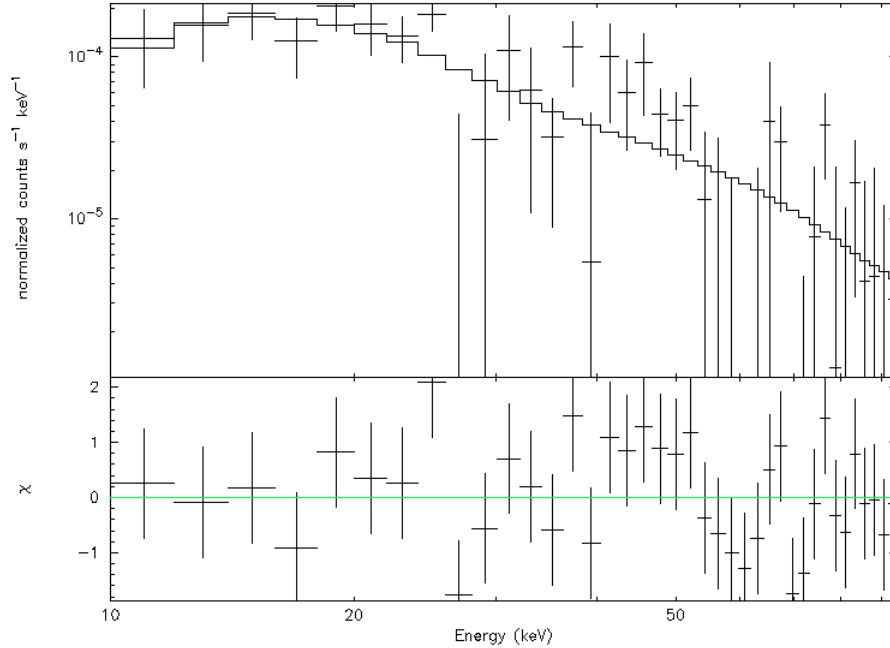
BAT spectrum and χ^2 residuals for GRB091029. XSPEC analysis allows to choose among several fit models and also reports fit parameters and χ^2 value. For this spectrum, power law model has been used.

3.1.1.3 Sky image

The same procedure used for creating detector plane image provides sky images. As BAT energy range lays from 15 to 350 keV, images over any energy band into this interval can be obtained. Scheme is the following: a DPI is created, then it is deconvolved by FFT applying weighted mask previously created. Terminal commands are the following:

- *>batbinevt detmask=grb.mask*
  This command allows to create DPI file. User is requested to enter input and output file names: here, input file is **uf.evt,* located in *../bat/event* directory; output name is *grb_4.dpi* because 4 different energy ranges have been chosen. If script works well, following message appeare at the end of batbinevt environment:
  DPIs written to grb_4.dpi

- $>$*batfftimage detmask=grb.mask*
  This command performs FFT of **.dpi* file. If script works well, this line
  appears at the end of batfftimage environment:
  Sky image # written to grb_4.img
  where # stands for energy range number $(1-4$ in this case).

3.2   XRT analysis

XRT analysis tools are both specific for X-ray data reduction, that is XTRDAS,
and generic tools like FTOOLS. User can work directly with second level data
to produce his own results. However, it is highly recommended to start from
one level unscreened data, running *xrtpipeline* script:
  $>$ *xrtpipeline [createexpomap=yes cleanup=no]*
  User are requested to enter object coordinates and input and output direc-
tory name. Pipeline products are stored in output directory. Usually, it has
the same input directory name, followed by *-xrt*. Command in brackets are ad-
ditional: *createexpomap* creates an exposure map for each event, while *cleanup*
allows to keep or delete temporary pipeline files.
  Once *xrtpipeline* has been run, second level data analysis can be performed.
It follows the steps listed below:

- Source detection and position determination. This step allows to select
  the source among all the detected events in the same field of view and to
  determine its position with high precision.

- Extracting images. Sky images can be obtained for different energy ranges
  and for different available modes, such as WT (1D image) and PC (2D
  image).

- Extracting spectra and light curves. Spectra have to be prepared before
  viewing them in XSPEC, that is correct binning size and count rate have
  to be set. Light curves can be shown using *XCRONS* or other FTOOLS
  software.

Crucial role in XRT data reduction is played by *XSELECT:* it is a command
line interface and it is used to extract images, light curves and spectra from
level 2 XRT data.

3.2.1   XRT pipeline

In this section, XRT scripts and results are reported. A complete and under-
standable guide can be found at UK Swift website [5].

3.2.1.1   Source detection

Source detection involves use of *XIMAGE* interface. Typing the following com-
mand:

> *ximage*

user is requested to enter **posk.img* filename, located in *00NNNNNN000-xrt* directory. A window is soon opened and entire field of view is shown, in detector coordinates (that is pixel units).

FOV image and source zoom are reported below. Here source determination is very easy, due to extreme source brightness. Sometimes, to run *sosta* command in the same shell is necessary, as many afterglow sources can be confused with other point sources.
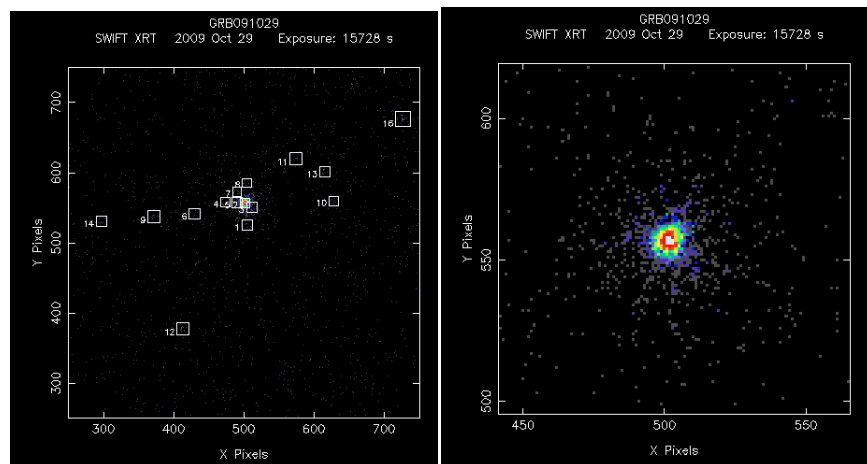
XRT field of view (left) and source image. Color scale is proportional to brightness scale (white for the brightest region). XIMAGE has identified several X-ray sources. However, in this case GRB afterglow is particularly bright, so it can be chosen without doubt. In fact, running sosta *command, signal to noise ratio of* 41.1 *is shown as a result.*

Source position can be obtained running *xrtcentroid* command. It is necessary to quit *XIMAGE* interface. As command has been entered, a new *XIMAGE* environment appears: selecting source centre, RA and DEC coordinates in degree are shown on terminal.

3.2.1.2 Extracting images

In this section, both WT and PC mode images are reported. To run *XSELECT* requires very easy commands. User is requested to enter input file name (which is *sw00NNNNNN000xwtw2po_cl.evt* or *sw00NNNNNN000xpcw3po_cl.evt* depending on what mode has been used). A *XSELECT* environment is opened and many tools can be used to modify source image. It is also possible to set a user-defined energy range with the following command:

> *filter pha_cutoff # #*
> *extract image*
> *save image #-#keV.im*

> *clear pha_ cutoff*

where # stands for minimum and maximum energy range value. It is important to notice that extremal values have to be entered as channel value, each channel counting for $10\,eV$.

WT and PC mode images are shown below.
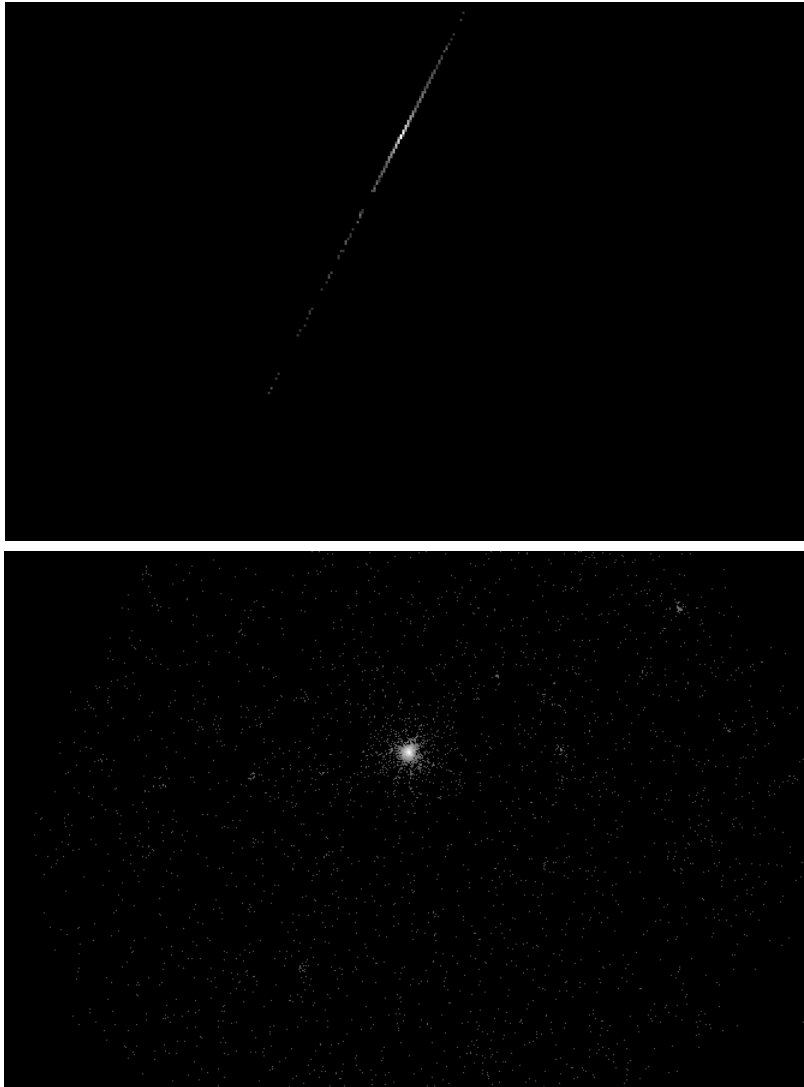
XRT source images for GRB091029. WT mode image is shown on the top: it is clear how this mode is able to perform just a 1D image. The bottom plot is a PC mode, 2D image: both source and background are evident. Logarithmic scale and zoom1 tools have been set.

3.2.1.3   Extracting spectra and light curves

XSELECT plays again a crucial role. In this section, only PC mode data are used as an example. To extract both spectrum and light curve, it is requested to extract source image previously and to save source and background region. This can be done pointing cursor and selecting circular regions. Double clicking on them, user can set their radius. Usually, it a good choice to set source radius at a half of background radius. Once both regions have been saved, user can extract spectrum from them, typing the following lines:

> *filter region *.reg*
> *extract spectrum*
> *save spectrum *.pi*

where * stands for file name.

Once spectra have been extracted, they have to be corrected to run into *XSPEC.* For this purpose, exposure map and Ancillary Response Files (ARF) need to be created. Exposure map is already saved in *-xrt* direcory, if user set *createexpomap=yes* at the beginning of *xrtpipeline.* ARF are created with the following script:

>*xrtmkarf expofile=sw00NNNNNN000xpcw3po_ ex.img*

User is requested to enter input and output filenames. Here, input file is *.pi* one, while output file is *.arf.*

XRT spectrum and χ^2 residuals for GRB091029 are reported below.
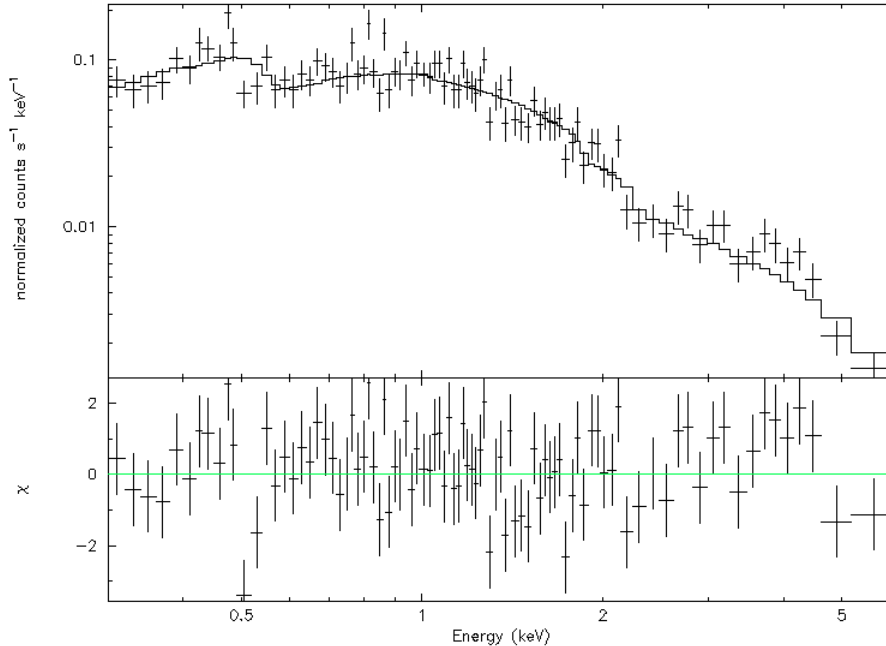
XRT fitted spectrum and χ^2 residuals for GRB091029. Multiplicative model has been used for fitting data. In particular, absorption model times power law model.

XSELECT also allows to extract a light curve, running the same script for extracting spectrum, but for setting *lc* extension in output file name. Using the command *filter cursor time,* user can additionally set the time interval for the light curve. Here, the first snapshot is chosen and *GRB*091029 light curve for early X-ray emission is reported below.
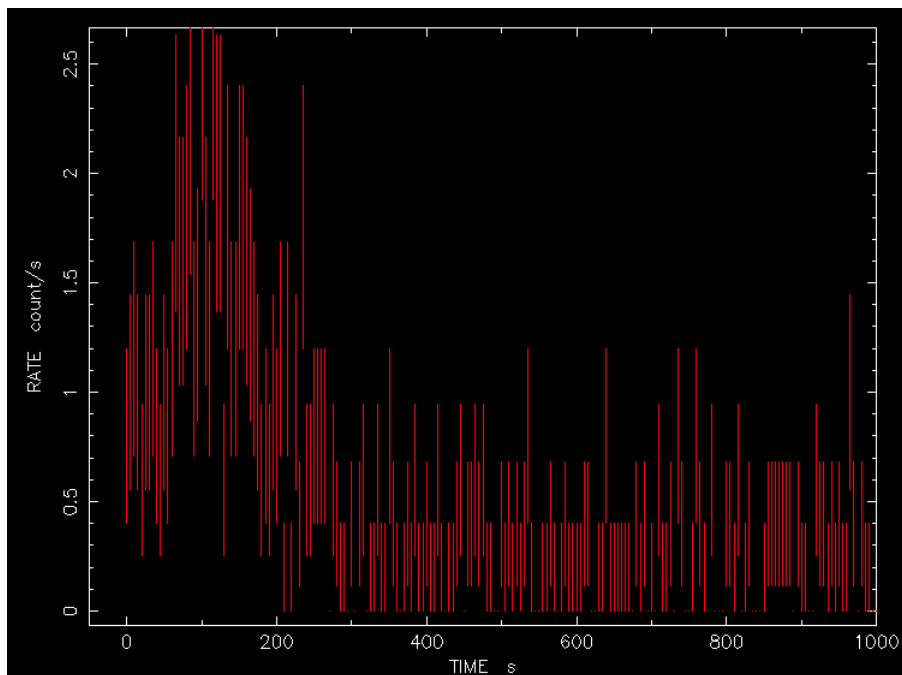
*XRT light curve for GRB*091029. *Time range belongs to the early emission.*

To view light curves, *XRONOS* interface can be used (it is part of FTOOLS package). However, the previous graph has been viewed in *fplot.*

Part II

Data analysis

Chapter 4

Sample choice and classification

In this second part, summer project work is explained in detail. In this chapter, sample choice and its classification are described. Chosen GRBs list (Table 1) and their classification lists (Table 2) are reported in Appendix.

4.1 Known redshift GRBs

Chosen sample is composed by all the known redshift GRBs detected from January 2005 ($GRB050126$) to July 2011 ($GRB110715A$). It is a hundred-event sample, so it allows to conduct statistical analysis. To know redshift is a key, because long term goal should be to use GRBs as cosmological tools, identifying correlation between their intrinsic properties and distance.

For this work purpose, redshift has allowed to correct observational light curves (flux versus laboratory time) for relativistic time delay and luminosity distance, switching to theoretical curves (luminosity versus source time). In addition, redshift distribution has been useful to exclude any distance selection effects.

GRBs label and their redshift have been read from GCN circulars [7].

4.2 Classifying light curves

GRBs are unique events, no GRB is similar to another. As a result, try to classifying GRBs light curves is a complicated issue. The easiest thing to do is looking light curves and try to find some common shapes just by eyes.

This work first step has been to define a BAT light curves classification. At first glance, it should be accepted that BAT light curves show four different shapes:

- Single pulse shape

- Double pulse shape

- Multi pulse shape

- Two-well-separated-event shape

Examples of each of the previous items are reported below.
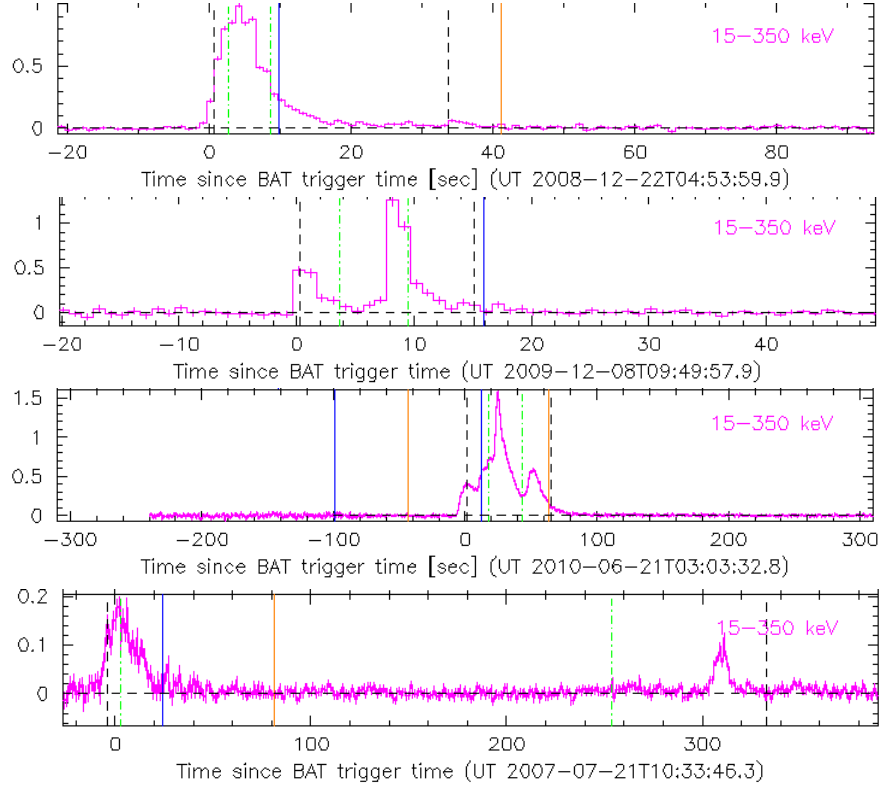
Examples of the previous classification items. From top to bottom, single peak, double peak, multi peak and two-well-separated-event shapes.

As BAT classification has been completed, XRT light curves [6] have been plotted, in order to identify any correlation between BAT curve shape and XRT curve behavior. It is known [9], actually, that a positive correlation between BAT light curve shape and brightness exists. However, possible afterglow correlations have not been examined yet. The following plot shows first result obtained from previous raw classification. It seems pretty encouraging. In particular, different groups brightness catches observer eyes (multi structured GRBs seem to be brighter), while, looking more accurately, different groups slope behavior can be recognized (single pulse group seems to show a constant decrease; in contrast, multi structured GRBs have a broken slope, becoming steeper at late times).
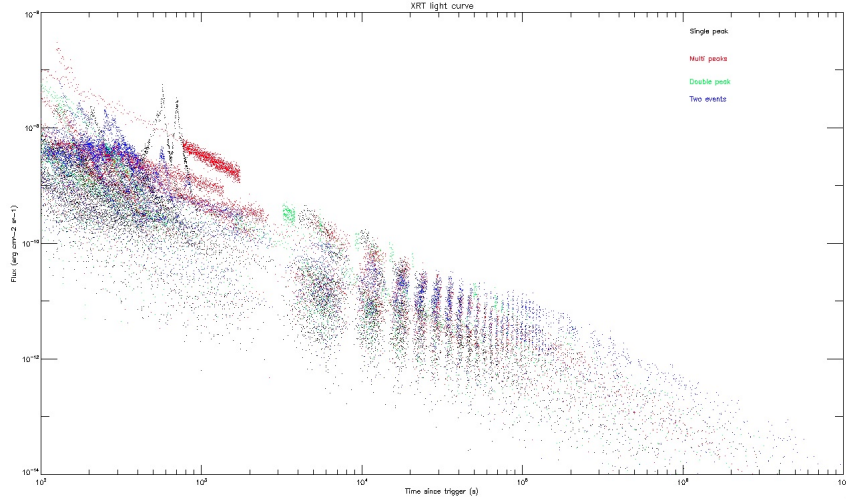
XRT flux versus laboratory time since BAT trigger. Different colors correspond to different BAT curve shapes, as legend in top right shows. Although raw classification and no redshift corrections, this plot clearly shows a possible correlation between BAT curve shape and XRT curve behavior.

However, need for more quantitative result requires to be very clear about classification rules. Looking BAT light curves more carefully, it pops up that some curves are too faint to be distinguished and classified. Furthermore, distinction between double pulse and multi pulse groups is often hard to declare. For this reason, final classification is composed by the following three items:

- Clear single pulse event, well fitted by a Fast Rise Exponential Decline (FRED) curve

- Multi structured events, considering all the bursts showing more than one peak

- Two-event bursts, separated by more than hundred seconds

Additionally, to require a cutoff at low energy for BAT curves allows to exclude too faint and indistinguishable events. For this purpose, $1\,s$ BAT peak flux has been stored for each event. Then, cutoff level has been put just below the last faint still distinguishable curve. It corresponds to $0.5\,photon\,cm^{-2}\,s^{-1}$. It helps avoid mistakes in classifying an event as single pulse or multi pulse one. Two-event bursts, being very peculiar and well defined, do not need any cutoff.

Classification lists are reported in Appendix (Table 2). An indistinguishable event example is shown below.
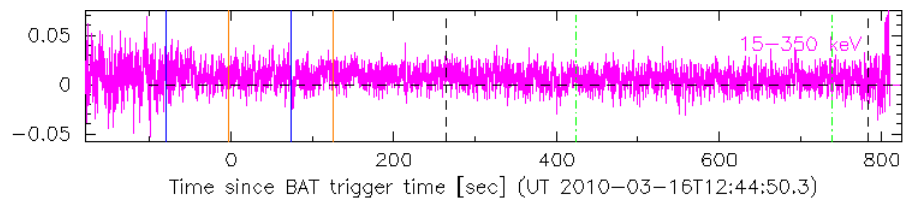
Indistinguishable event example. Burst is too faint to be separated from detector noise and to be assigned to any classification groups. Cutoff allows to exclude such events.

It has to be stressed that classification groups size is not the same. Multi structured group is the most populated, with almost 70 events, while two-event group is composed just by 12 bursts. Single pulse group size is almost half of multi pulse one. Despite not allowing to compare trends in bursts distribution within each group, this choice seemed more consistent for this work analysis. Another choice could be to use a different cutoff for each group, but that issue has been excluded by consistency reason: to make the same cutoff leads to more uniform samples, though they are not equally sized.

Chapter 5

Results

In this chapter, final results from XRT light curves analysis are described. Obviously, this work should be just the first step of a more refined analysis, which could lead to more valuable results on scientific point of view.

5.1 Redshift analysis

5.1.1 Light curve corrections

In order to discuss light curves intrinsic properties, redshift corrections are requested. In other words, there is need for switching from observational light curve, which is a flux versus laboratory time plot, to theoretical light curve, that is a luminosity versus source time plot.

X axis corrections are two, actually. One correction is about t_0 (light curve starting time) definition: BAT instrument sets t_0 after having determined event importance, in other words after having detected a significant increase in flux. So, BAT trigger time often does not correspond to t_0. GCN circulars report t_{100} starting time (100 subscript stands for time interval including 100% flux): this time has to be algebraically subtracted from X axis data set, in order to shift it to the correct initial time.

The other correction is a cosmological issue: GRBs have non-zero redshift, so time t_{obs} measured from observer does not correspond to source time t_s (they correspond each other if $z = 0$). More in detail, source time is stretched because of non-zero scale factor a. As relation between scale factor and redshift is the following

$$\frac{a(z)}{a(0)} = \frac{1}{1+z} \tag{5.1}$$

source time is related to observer time by

$$t_s = a(z) \, t_{obs} = \frac{t_{obs}}{1+z} \tag{5.2}$$

In conclusion, whole correction involving X axis data set has been obtained via the following equation

$$t_s = \frac{(t_{obs} - t_{100})}{1 + z} \tag{5.3}$$

Y axis correction involved converting flux to luminosity. As flux is energy flowing through unitary area per second and luminosity is energy rate, standard conversion formula is the following:

$$L = 4\pi d^2 F \tag{5.4}$$

where d is source distance from observer. However, cosmological issue requires a more detailed analysis: because of non-zero scale factor, observed luminosity L_{obs} does not correspond to source luminosity L_s. In fact, photon wavelength is stretched by Universe expansion, resulting in energy decrease according to the following formula

$$h\nu(a) = \frac{h\nu_{obs}}{a} \tag{5.5}$$

In addition, previous time dilatation has to be taken into account. As a result, observed luminosity is related to source luminosity via the following formula

$$L_s = (1 + z)^2 L_{obs} = 4\pi(1 + z)^2 d^2 F = 4\pi d_L^2 F \tag{5.6}$$

where d_L, luminosity distance, represents cosmological corrections.

The second Y axis correction is known as *K-correction*. It is an astronomical correction, due to limited band of observation: flux measurements lay within $0.3 - 10\,keV$. If bolometric flux is measured, *K-correction* is not required. The correction amount is given by the following formula

$$L_s = (1 + z)^{\Gamma - 2} L_{obs} \tag{5.7}$$

where Γ is the photon index, obtained as light curve fit parameter. In conclusion, whole Y axis correction is summarized by this relation

$$L_s = (1 + z)^{\Gamma - 2} 4\pi d_L^2 F_{0.3 - 10\,keV} \tag{5.8}$$

All of the previous conversions, as all of the graphs reported in this paper, have been implemented via IDL scripts.

5.1.2 Redshift distribution

Another thing that should be taken into account is redshift distribution. In fact, conclusions strongly depend on possible redshift bias. For this reason, histograms of redshift for each classification group have been made. Final plots are reported below.
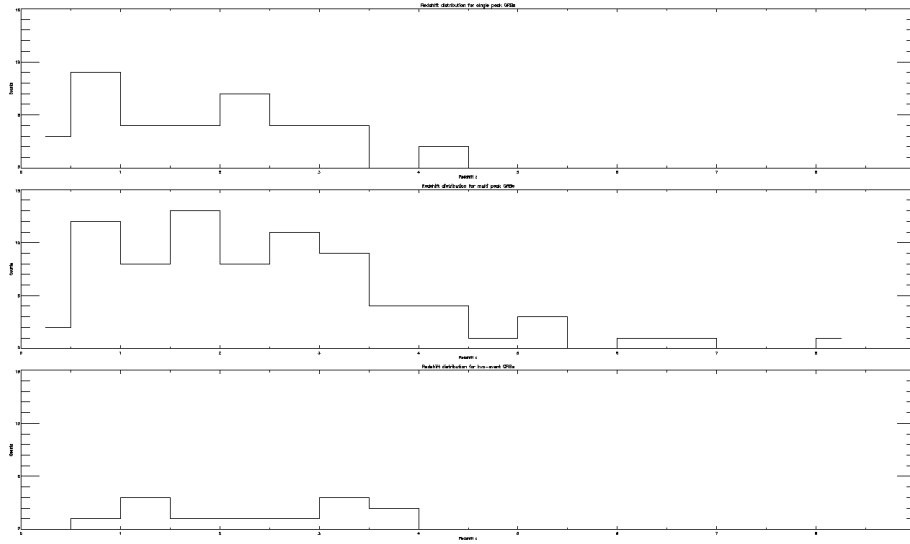
Comparison among redshift distribution for the three classification groups. From top to bottom, single pulse, multi pulse and two-event. It is clear that sample is not redshift-biased, as redshift distributions can be fitted by same shape and eventually overlapping curves.

The previous plot clearly excludes any bias arguments. Redshift distributions overlap each other almost perfectly. It has been taken into account that sample size is not the same, so the few higher redshift events in multi pulse distribution should be considered a faint tail due to this group size.

Maybe two-event distribution should be discussed more in detail. It appears that two-event bursts are high redshift phenomena, that is no more than one event with $z < 1$ has been detected. Unfortunately, the very limited size of this sample does not allow precise statistical analysis and, at this level, this interesting feature should be also explained as a size bias.

5.2   XRT light curves

As axis corrections have been made, light curves are ready to be plotted. The following plot shows theoretical XRT light curves. Each BAT group is represented by a different color.
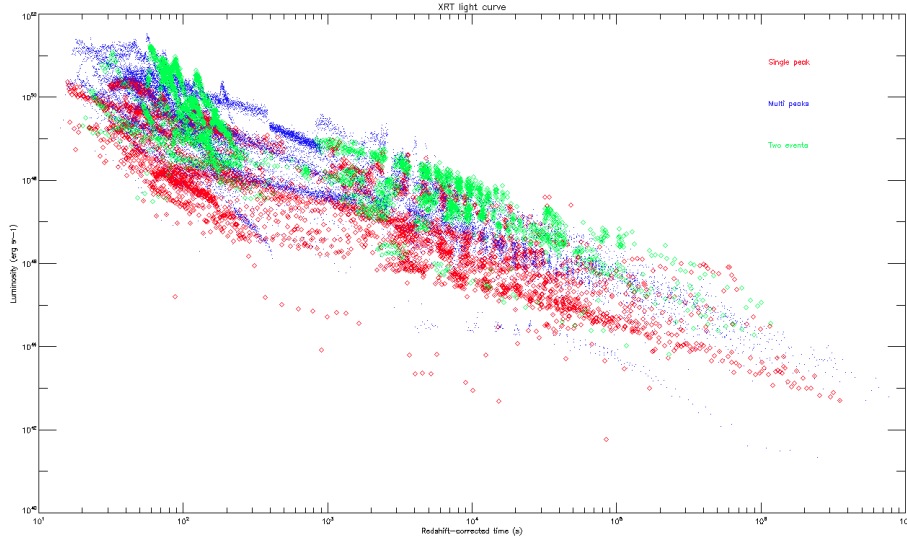
Theoretical XRT light curves. Each color represents a different classification group: red for single pulse, blue for multi pulse, green for two events. Red and green symbols are bigger than blue ones because of the limited sample size. Different curve shapes emerge clearly from this plot.

Initial raw result is confirmed here: BAT classification clearly has lead to different XRT groups. In detail:

- Multi structured events appear brighter than single pulse events, especially for early times. Two-event curves are also very bright.

- Single pulse events show a general steady slope, while multi pulse curves appear to be composed by two power law decays. In particular, at early times a shallow slope could be seen; in contrast, slope becomes steeper at late times. This different behavior allows the two groups to overlap at late time, where brightness distinction is no more observed.

- Two-event curves have a particular shape, with initial flairs, a significant time lag at $2\,10^2s < t < 8 - 9\,10^2s$ and a steady final decrease.

- Both single pulse and multi pulse curves show no break points. In fact, curves seem to continue also for time later than ones reported in the graph above. In contrast, a break point could be found for two-event curves. Qualitatively, it could be situated at $t = 10^5s$.

To be more quantitative, histograms of luminosity at certain times have been made. Three times have been chosen: $t_1 = 10^3s$, $t_2 = 10^4s$, $t_3 = 10^5s$. They ideally correspond to early, middle and late part of curves, respectively. Data before t_1 have been excluded, as that range is too close to prompt emission,

while this work focused on afterglow, and it often includes flairs, which are difficult to interpolate.

Obviously, data set does not include luminosity values corresponding exactly to previous times. So far, interpolation method has been necessary. The followed method uses a power law model to interpolate points and is based on two assumptions:

- interpolation is not performed among the entire data range, but choosing a limited time range (including one of the three times of interest, at least), as it could be well fitted by a simple power law model

- in case one or more of the three times falls within a gap (it is not so rare, as gaps occur between two satellite orbits), interpolation is performed between the two closest points including that time.

Although this method could appear rough, errors related to more refined model (such as using smoother functions) are not so better than this very simple's ones.

Final histograms are shown below.
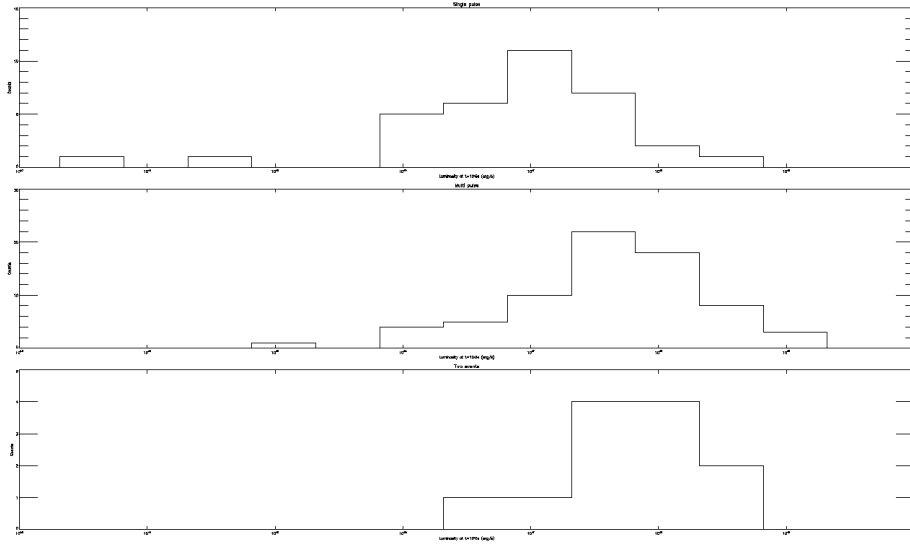
Luminosity distribution at $t_1 = 10^3 s$ for the three classification groups. From top to bottom, single pulse, multi pulse and two-event. X axis ranges from $10^{43} erg\, s^{-1}$ to $10^{50} erg\, s^{-1}$.
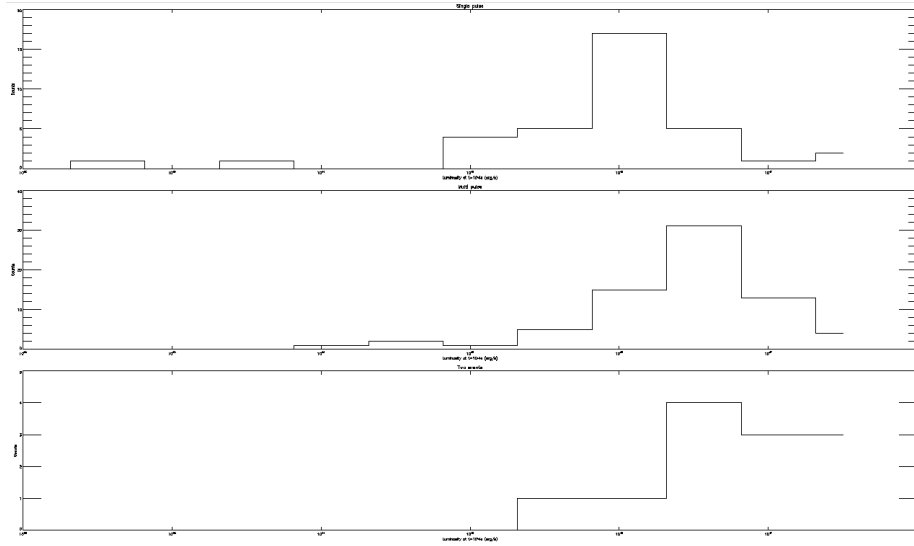
Luminosity distribution at $t_2 = 10^4 s$ for the three classification groups. From top to bottom, single pulse, multi pulse and two-event. X axis ranges from $10^{42} erg\,s^{-1}$ to $10^{48} erg\,s^{-1}$.
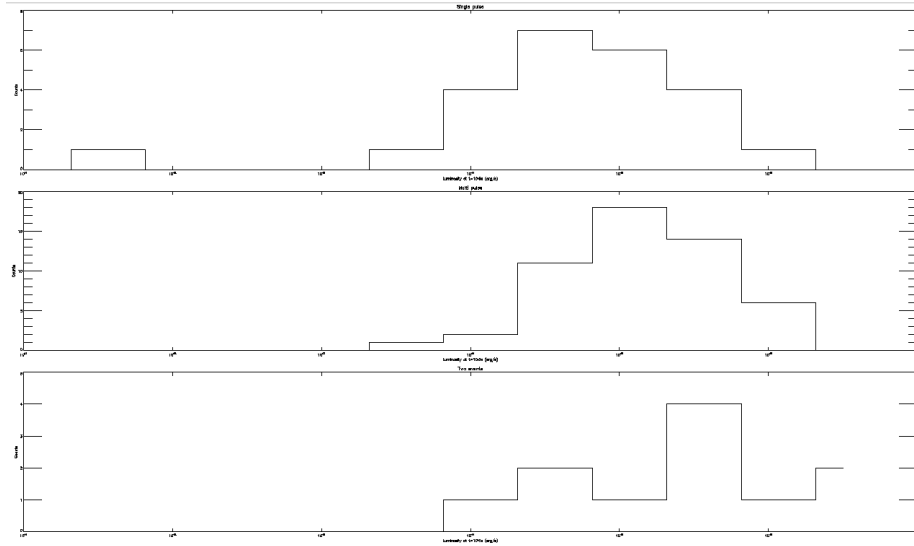
Luminosity distribution at $t_3 = 10^5 s$ for the three classification groups. From top to bottom, single pulse, multi pulse and two-event. X axis ranges from $10^{41} erg\,s^{-1}$ to $10^{47} erg\,s^{-1}$.

Qualitative clues are here confirmed. Considering first plot, it is clear how luminosity distribution shapes are pretty different and do not overlap each other.

They are distinctly peaked at diverse luminosity values, being multi pulse distribution brighter than single one. Two-event histogram also is situated close to the X axis upper bound.

At t_2, the previous feature is repeated, but now shapes look more similar and peaks tend to become closer and closer. Two-event distribution continue to miss fainter events.

So far, these two plot underline how the three histograms lay on different luminosity range, being two-event one the most narrow.

Final plot shows what has been summarized at the end of the second bullet point, just below light curves plot: distributions perfectly overlap each other and no significant peak differences are still evident. Finally, all the three histograms lay on the same range, including two-event one. While former distributions are more narrow close to their peak and show long tails, the latter ones appear smoother, broader and free of tails.

Chapter 6

Conclusion

This work has demonstrated a positive correlation between BAT light curves, that is prompt GRB emission, and XRT light curves, corresponding to GRB afterglow. In addition, it has provided important and interesting clues about intrinsic XRT light curves properties.

Firstly, a statistically significant sample has been chosen among all of the known redshift GRBs. Short GRBs and faint (and undistinguishable) events have been excluded, the latter one on BAT $1s$ flux base.

Then, sample has been classified by looking up BAT light curves: events have been divided among three groups, such as single pulse, multi pulse and two-event bursts. So far, a XRT light curves plot has shown significant differences in brightness and shape among the three groups.

Next step has been to correct data set for redshift and to scale X axis for the exact BAT trigger time. This step has allowed to switch from observational light curves (flux versus laboratory time) to theoretical ones (luminosity versus source time). Corrections have been necessary as this work is dealing with intrinsic curves properties: all possible bias issues have to be excluded. Being uniform, distribution of redshift for the three groups eventually shows no distance bias.

As corrections have been performed, theoretical light curves plot has confirmed previous raw results. Finally, histograms of luminosity at three different times (early, middle and late range, ideally) have quantified differences in XRT brightness.

In conclusion, a BAT-light-curve-shape-based classification allows to identify important features in the afterglow region. In detail:

- multi pulse events are brighter than single pulse bursts. In addition, the former ones show a broken power law shape, being shallow at the beginning and becoming steeper at later times; the latter ones appear to maintain a steady shape along the whole time range. Due to this feature, the two groups match at late times.

- two-event bursts are as bright as multi pulse ones. Their light curves show a peculiar trend: initial flairs, a significant gap between $10^2 s$ and $10^3 s$, a

33

steady final shape with an apparent cutoff at $10^5 s$. All of them also seem to be far events, missing more than one $z < 1$ burst. However, the small sample size does not allow statistically significant analysis.

Time reasons have excluded the possibility to conduct a more quantitative analysis about light curves shapes. So far, this work has been focused on XRT light curves brightness, being very qualitative about shapes. Next step should be to fit light curves, using power law models, in order to discuss photon index distributions and possible cutoff. Finally, to try to expand two-event sample size could allow to obtain interesting clues about this very peculiar classification group.

Chapter 7

Appendix

In this section, list of sample GRBs and classification groups are reported.

The first list collects all the known redshift GRBs. However, some of them were excluded from data analysis, as either they belong to Short GRBs groups or their BAT light curve are too faint and undistinguishable.

All of the analyzed events are reported in classification lists. Single pulse and multi pulse lists also include BAT $1\,s$ peak flux.

7.1   Table 1 - Known redshift GRBs

Known redshift GRBs from the 26th of January, 2005 to the 15th of July, 2011.

GRB label	Redshift z	GRB label	Redshift z
		090418A	1.608
110715A	0.82	090417B	0.345
110213A	1.46	090423	8.26
110106A	0.093	090313	3.375
110128A	2.339	090205	4.6497
100901A	1.408	090102	1.547
100816A	0.8035	081222	2.77
100621A	0.542	081203A	2.05
100425A	1.775	081121	2.512
100316D	0.059	081118	2.58
100302A	4.813	081109A	<3.5
100206A	0.41	081029	3.847
091208B	1.063	081028	3.083
091029	2.752	081008	1.9685
091127	0.49	081007	0.5295
091109A	3.5	080928	1.6919
091024	1.092	080916A	0.6887
091020	1.71	080913	6.7
091018	0.971	080905B	2.3739
090926A	2.1062	080805	1.5042
091003	0.8969	080804	2.2045
090927	1.37	080810	3.3604
090902B	1.822	080721	2.602
090926B	1.24	080710	0.8454
090814A	0.696	080411	1.0301
090812	2.452	080707	1.23
090809A	2.737	080607	3.0368
090726	2.71	080603B	2.6892
090715B	3.0	080605	1.6398
090618	0.54	080604	1.4171
090516	4.109	080520	1.5457
090529A	2.63	080516	3.2
090424	0.544	080514B	1.9<z<3.7
090519	3.85	080330	1.5119
090510	0.903	080413B	1.1014
090426	2.609	080413A	2.433

GRB label	Redshift z
080319C	1.9492
080319B	0.9382
080310	2.4274
080212	<3.5
080210	2.6419
080205	4.0
080129	4.349
071122	1.14
071117	1.3308
071112C	0.8227
071031	2.6918
071025	5.2
071020	2.1462
071010B	0.947
071003	1.60435
070810A	2.17
070802	2.4541
070724A	0.457
070721B	3.6298
070714B	0.923
070611	2.0394
070529	2.4996
070506	2.3090
070419A	0.9705
070411	2.9358
070318	0.8397
070306	1.4965
070208	1.165
070110	2.3521
061222B	3.355
061222A	2.088
061217	0.827
061210	0.4095
061126	1.1588
061121	1.3145
061110B	3.4344
061110A	0.757
061021	0.3463
061007	1.2622
061006	0.4377
061004	3.3, 0.3
060927	5.4636
060926	3.2086
060912A	0.937
060908	1.8836
060906	3.6856
060904B	0.7029

060814	0.84
060729	0.5428
060714	2.7108
060708	1.92
060707	3.424
060614	0.1257
060607A	3.0749
060605	3.773
060526	3.2213
060522	5.11
060512	2.1
060510B	4.941
060505	0.089
060502A	1.5026
060418	1.4901
060223A	4.41
060218	0.03342
060210	3.9133
060206	4.0559
060124	2.3
060115	3.5328
051221A	0.5465
051111	1.55
051109A	2.346
051016B	0.9364
050922C	2.1995
050908	3.3467
050904	6.295
050826	0.296
050824	0.8278
050820A	2.6147
050814	5.3
050802	1.7102
050801	1.38
050730	3.9693
050724	0.258
050603	2.821
050525A	0.606
050509B	0.226
050505	4.275
050416A	0.6528
050401	2.8983
050319	3.2425
050318	1.444
050315	1.95
050223	0.584
050126	1.29

7.2 Table 2 - Classification lists

Single pulse bursts	
GRB label	$1\,s\,peak\,flux\,(ph\,s^{-1}cm^{-2})$
090809A	1.080
050922C	7.040
110128A	0.753
090313	1.090
070810A	1.890
060926	1.100
070611	0.729
070506	0.949
060512	0.883
050908	0.698
081118	0.607
081109A	1.430
080129	0.550
100816A	10.800
091018	9.550
081222	7.440
080805	1.040
080804	3.070
080710	0.926
080430	2.650
080413B	18.000
071117	11.000
071031	0.544
071010B	7.290
070714B	2.720
070318	1.640
061021	6.120
061004	2.480
060912A	8.270
060708	1.910
060203	0.572
051111	1.840
050801	1.460
050724	3.390
050416A	4.770
091018	9.55
081007	2.85
110726A	1.01
110106A	1.80
090927	1.84

Multi pulse bursts		GRB label	$1\,s\,peak\,flux\,(ph\,s^{-1}cm^{-2})$
GRB label	$1\,s\,peak\,flux\,(ph\,s^{-1}cm^{-2})$	060707	1.080
100621A	12.500	060614	11.500
091208B	14.700	060510B	0.574
091127	41.700	050603	15.300
091024	2.080	050525A	41.000
091020	4.180	050505	1.850
090812	3.560	080319B	25.100
090618	38.000	071025	1.640
090424	69.500	061007	14.700
081203A	2.810	060502A	1.740
080928	2.080	050315	1.890
080916A	2.620	080913	1.370
080607	23.200	051016B	1.280
080605	19.600	050904	0.639
080516	1.700	050223	0.650
080413A	5.400	110213A	1.560
080319C	5.080	051109A	3.890
080212	1.130	090814A	0.547
080210	1.590	090519	0.570
080205	1.410	060522	0.538
091127	41.700	091109A	1.230
091029	1.720	050802	2.680
090926B	3.190	050730	0.562
090102	5.370	110731A	11.0
090726	0.738	100816A	11.0
090423	1.730	060223A	1.35
090418A	1.910	090516	1.73
071020	8.390	110818A	1.57
070411	0.928	081008	1.30
070110	0.616	060908	3.09
061222B	1.510	080905B	1.66
061222A	6.440	060729	1.14
061126	9.770	060714	1.27
060927	2.680	100425A	1.36
060607A	1.400	080330	0.961
060418	6.580	090715B	3.72
081121	3.460	071003	6.40
080810	2.000	081028	0.576
080721	18.100	080603B	3.54
080707	1.070	080310	1.32
060906	1.990	060115	0.862
060814	7.260	050401	11.2

It has to be underlined that no cutoff has been performed for two-event group, as this kind of events are very distinguishable respect to the others. So far, only GRB label is reported for this group.

Two-event bursts
GRB label
070721B
060904B
100901A
060526
070306
061121
060210
050820A
050319
080310
080928
090715B

Bibliography

[1] Piran, T., *The Physics of Gamma Ray Bursts,* Rev. Mod. Phys. 76: 1143-1210, 2004

[2] Xiao, L., *Gamma Ray Burst Redshift Catalog and Applications,* dissertation for Ph.D. degree in Physics and Astronomy department, 2010

[3] Wikipedia, *http://en.wikipedia.org/wiki/Gamma-ray_burst*, 2011 (last update)

[4] ASD, GSFC, *http://swift.gsfc.nasa.gov/docs/swift/about_swift/,* 2010 (last update)

[5] UK Swift website, *http://www.swift.ac.uk/proc_guide.shtml,* 2011 (last update)

[6] UK Swift wepsite, *http://www.swift.ac.uk/results.shtml,* 2011 (last update)

[7] ASD, GSFC, *http://gcn.gsfc.nasa.gov/,* 2011 (last update)

[8] ASD, GSFC, HEAs Division, SAO, *http://heasarc.gsfc.nasa.gov/cgi-bin/W3Browse/swift.pl*

[9] Reichart, Daniel E. et al., *A Possible Cepheid-like Luminosity Estimator for the Long Gamma-Ray Bursts,* ApJ, 552, 57

[10] Arnaud, K.A., 1996, *Astronomical Data Analysis Software and Systems V* , eds. Jacoby G. and Barnes J., p17, ASP Conf. Series volume 101*, http://heasarc.gsfc.nasa.gov/docs/xanadu/xspec/index.html*